AIAA JOURNAL
Vol. 49, No. 6, June 2011

Comparison Between Postprocessing Methods Applied to Rotor–Stator-Interaction Tone-Noise Problems

Davide Giacché* and Liping Xu†
University of Cambridge, Cambridge, England CB3 0DY, United Kingdom
and
John Coupland‡ and Alexander G. Wilson§
Rolls-Royce, plc., Derby, England, DE24 8BJ, United Kingdom

DOI: 10.2514/1.J050523

The range of applicability and accuracy of the major postprocessing methods available today to extract tone-noise information from unsteady aerodynamic source data for the rotor–stator-interaction problem are systematically examined using four numerical examples of increasing geometric and flow complexity. The test cases span from the benchmark problem of a vortical gust impinging on an unloaded cascade of flat plates to a fan stage representative of a modern turbofan engine. A linearized Navier–Stokes computational fluid dynamics method is used to obtain the aerodynamic solutions for the tone-noise postprocessing. The underlying assumptions of each postprocessing method are examined, highlighting the shortcomings and the strengths of each method. In particular, the effects of the duct geometry and mean flow are investigated. An acoustic analogy integral method, and various wave-splitting techniques are considered. Furthermore, the influence of the nonuniformity and swirl that characterize the mean flow in a real fan stage on the sound power conservation is examined using a modal expression of the sound power for nonuniform swirling flows in the high-frequency limit. A comparison with the widely used expression of the sound power for a uniform flow is also carried out.

Nomenclature

A_{mn}	=	modal amplitudes
B	=	number of blades
b	=	blade chord
c	=	speed of sound, m/s
f	=	generic function defining the blade surface
G	=	Green function
$H(f)$	=	Heaviside function
$\mathbf{H_m}$	=	Fourier transform of the computational fluid dynamics solution of order m
$\mathbf{I}$	=	energy flux vector, W/m^2
k	=	axial wave number, m^{-1}
M	=	Mach number
m	=	circumferential wave number, modal index
n	=	modal index
$\mathbf{n}$	=	outward unit normal vector
P_{mn}	=	eigenfunction of pressure perturbation
p	=	pressure, Pa
p_{ij}	=	compressive stress tensor
R_{mn}	=	eigenfunction of density perturbation
r	=	radial coordinate, m
T_{ij}	=	Lighthill's stress tensor
T_{mn}	=	eigenfunction of azimuthal velocity perturbation
t	=	time variable, s
U	=	mean axial velocity, m/s
u	=	disturbance fluid velocity, m/s
V	=	number of vanes
v_i	=	surface velocity, m/s
W	=	acoustic power, W
X_{mn}	=	eigenfunction of axial velocity perturbation
x	=	axial coordinate, m
$\delta(f)$	=	Dirac delta function
δ_{ij}	=	Kronecker delta
θ	=	azimuthal coordinate, rad
μ	=	radial mode order
ρ	=	density, kg/m^3
σ^2	=	standard deviation (used for the axial variation of sound pressure level or sound power level)
ϕ	=	phase shift
Ψ	=	slowly varying eigenfunctions
Ω	=	rotational speed, rad/s
ω	=	frequency, rad/s

Subscript

0	=	mean flow quantity

Superscripts

$*$	=	complex conjugate
$\pm$	=	upstream/downstream-propagating modes

Received 26 March 2010; revision received 29 November 2010; accepted for publication 21 January 2011.

*Whittle Laboratory, Department of Engineering, 1 J. J. Thomson Avenue; dg305@cam.ac.uk.
†University Lecturer in Turbomachinery, Whittle Laboratory, Department of Engineering, 1 J. J. Thomson Avenue.
‡Aerothermal Methods Specialist, P.O. Box 31, Derby. Member AIAA.
§Chief of Hydrodynamics CFD—Marine, P.O. Box 31.

I. Introduction

THE application of computational fluid dynamics (CFD) methods to the investigation of aerodynamic and acoustic phenomena occurring in a modern jet engine can provide the turbomachinery designer and the noise engineer with invaluable information, which can then be used to improve the design or to assist experimental campaigns. To this effect, it is vital to be able to extract the relevant information in a consistent and reliable way, and to understand the limits and the implications of the assumptions at the base of the postprocessing techniques in use. Motivated by this consideration, the application of two major classes of methods in use today for the extraction of tone-noise information from the CFD aerodynamic source data for the rotor–stator-interaction problem will be systematically assessed in the present paper.

Two groups of methods are applied to the general wake/vane interaction noise problem, culminating in the analysis of a realistic fan/bypass outlet guide vane (OGV) configuration. The first group of methods is based on the *acoustic analogy approach*, which enables the prediction of the noise radiated by a rotating blade as an integral of the unsteady pressure fluctuations arising from the interaction between rotating and stationary blades. The second group of methods, commonly known as *wave-splitting* techniques, is based upon an eigenmode analysis of the unsteady flowfield and, as the name suggests, its primary aim is to split the unsteady flowfield into the incoming and the outgoing waves inside the computational domain.

A brief account of the underlying theory of the postprocessing methods used in the current work will be provided, and their strengths and weaknesses will be pointed out. In particular, the main advantages and disadvantages of the methods will be investigated by use of a range of numerical examples of increasing complexity, from the simple vortical gust/flat-plate interaction in an inviscid uniform ducted axial mean flow, to a realistic fan/OGV configuration. A linearized CFD approach is used throughout the paper to obtain the aerodynamic solutions that contain the tone-noise information.

For the fan/OGV test case, the approximation of the energy corollary in the high-frequency limit presented in [1] will be evaluated. The influence of the nonuniform swirling mean flow on the conservation of acoustic intensity will be investigated for upstream- and downstream-propagating acoustic waves generated by the impingement of the fan wakes on the bypass stator vanes. Furthermore, a comparison with the widely used expression of the sound power for a uniform mean flow will be carried out.

II. Methods Description

A. Acoustic Analogy Approach

The first method employed to derive tone-noise information from the linearized CFD solutions of the general rotor–stator-interaction problem makes use of the Ffowcs Williams–Hawkings (FW-H) equation [2]. An exhaustive description of the method is given in [3], and only the salient aspects will be outlined here.

In its current implementation the method is applied to a blade row in a uniform axial flow in an annular duct, i.e., with constant hub and tip radii, and is based upon a convective acoustic analogy equation for the case of a moving source in a moving medium [4]. If the motion of the surface source is described by $f(\mathbf{x}, t) = 0$, the Euler equations can be manipulated to obtain a convective wave equation for a nonporous surface of the form

$$\left(\frac{\partial^2}{\partial t^2} - c^2\frac{\partial^2}{\partial x_i^2} + 2U_{0x}\frac{\partial}{\partial t}\frac{\partial}{\partial x_1} + U_{0x}^2\frac{\partial^2}{\partial x_1^2}\right)H(f)\rho' = \left(\frac{\partial}{\partial t} + U_{0x}\frac{\partial}{\partial x_1}\right)\left[\rho_0(v_i - U_{0x}\mathbf{e_1})\frac{\partial f}{\partial x_i}\delta(f)\right] - \frac{\partial}{\partial x_i}\left[p_{ij}\frac{\partial f}{\partial x_j}\delta(f)\right] + \frac{\partial^2}{\partial x_i \partial x_j}(H(f)T_{ij}) \quad (1)$$

where c is the sound speed, ρ is the density, ρ' is the density perturbation, and the subscript 0 refers to the value of the variables in the undisturbed medium. Lighthill's stress tensor, T_{ij}, is defined as $T_{ij} = p_{ij} - c^2\rho'\delta_{ij} + \rho u_i u_j$, where u_i is the disturbance fluid velocity, p_{ij} is the compressive stress tensor, and δ_{ij} is the Kröeneker delta. In Eq. (1) the derivatives are to be interpreted as generalized derivatives, while $H(f)$ and $\delta(f)$ are the Heaviside and Dirac delta functions, respectively. The surface of the body is described by the equation $f(\mathbf{x}, t) = 0$ with f being defined such that $\mathbf{n} = \nabla f$ is the outward unit normal vector pointing into the fluid region $f > 0$ (Fig. 1). The symbol v_i in Eq. (1) is used for the velocity of the moving surface.

The right-hand side of Eq. (1) comprises the contributions of three major sources: a monopole source due to the blade thickness (first term), a dipole source, commonly known as *loading source*, due to the unsteady pressures on the blade surface (second term), and a nonlinear term due to quadrupole sources (third term). The first two terms represent surface sources and act only on the surface $f = 0$.

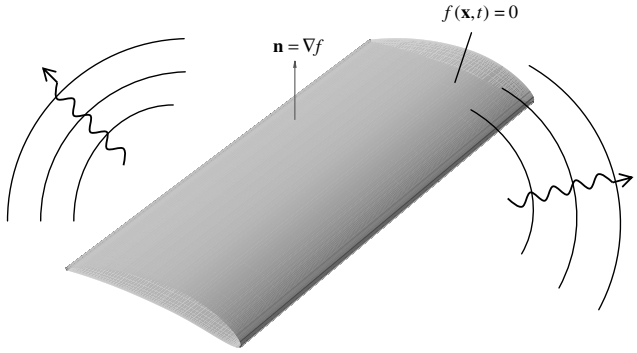

Fig. 1 Schematic of the vane surface $f(x, t) = 0$ and its outward normal vector.

The first term has the monopole character of a volume source distribution at the surface and is often referred to as *thickness noise* because it can be interpreted as the displacement by the moving body of the surrounding fluid. The pressure distribution in the second term presents a typical dipole character and can be associated with the force exerted by the moving body on the surrounding medium. The third term is a volume source and therefore acts throughout the volume $f > 0$.

The monopole contribution due to the displacement thickness of the blade can normally be ignored for subsonic tip speeds since only evanescent modes are generated in this case. The quadrupole sources can also be neglected in many subsonic applications, leaving the loading source as the dominant contribution.

Equation (1) with only the dipole (loading) source on the right-hand side can be solved using Green's function G for the convected wave equation in a hard-walled annular duct. This is made possible by a modal representation of G as a superposition of circumferential and axial waves [5]. The pressure field at any point inside the duct can be determined by integrating the unsteady pressure on the blade surface, generated by the impingement of the rotor wakes, using Eq. (2):

$$p(\mathbf{x}, t) = -\int_{-\infty}^{\infty}\oiint_{f=0} p(\xi, \tau)\nabla_\xi G(\mathbf{x}, t; \xi, \tau)\cdot\mathbf{n}(\xi, \tau)\,\mathrm{d}S\,\mathrm{d}\tau \quad (2)$$

In view of the modal nature of G, Eq. (2) can be used to determine the radiated noise in terms of uniform-flow duct modes. The surface integral expressed by Eq. (2) accounts for the three-dimensional nature of the unsteady pressure distribution over the vane surface and allows for the distortion of the incoming wake due to the nonuniform mean flow. The latter phenomenon can generate differences in amplitude and phase of the incoming wake experienced by the pressure and suction sides of the blades, and consequently modify the unsteady loading distributions on the blade surface [6]. The inclusion of these effects is an important aspect of the method, which sets it apart from the typical (simplified) application of the FW-H equation, where the vanes are modeled as zero-thickness flat plates, and the unsteady loading is often determined using 2-D strip theory. In the simplified approach, the vane geometry and unsteady loading depends upon radius only, greatly simplifying the integral in Eq. (2), but inevitably ignoring several potentially important features in the noise-generation process.

The acoustic analogy approach (AA) to the problem of computing the noise generated by rotor–stator interaction inside the fan duct has been shown to produce reasonable qualitative data-theory agreement [6,7], especially when the surface pressure distribution is accurately known for low to moderate tip fan speeds [6]. Three essentials elements are at the base of the approach and determine its range of applicability and accuracy: 1) the use of uniform-flow annular-duct Green's functions, 2) the precision with which the vane unsteady surface pressures are known and 3) the unsteady loading interpolation and integration over the blade surface.

When the blade unsteady pressures are known with a good level of accuracy, from experiments or 3-D CFD simulations, the duct and

flow characteristics can still influence the overall accuracy of the method. If the flow is significantly nonuniform, the theoretical basis for the use of uniform-flow Green's functions is not solid and this may induce errors in the noise level predictions. Also, even when the flow can be reasonably retained as uniform and the unsteady surface pressures are known with sufficient resolution and accuracy, any duct variation, particularly in the source region (i.e., the vane in a rotor–stator-interaction problem), can undermine the pressure integration and the modal expression of the unsteady pressure inside the duct.

The shift of the duct geometry and flow characteristics from the cylindrical annulus and uniform-flow assumptions may constitute important factors not just for the accuracy, but also for the reliability of an AA integral method to predict rotor–stator-interaction tone noise. The influence of the duct geometry and of a nonuniform swirling flow will be investigated in the results section of this paper for a series of numerical examples of increasing complexity.

B. Wave-Splitting Methods

The second group of methods in use today to extract tone-noise information from the aerodynamic source data goes under the name of wave-splitting techniques. The wave-splitting technique rests on the possibility of using a modal representation of the unsteady flow, and its objective is to decompose the unsteady flowfield into upstream- and downstream-propagating eigenmodes and differentiate between pressure-dominated (acoustic), and nearly convected modes.

In uniform flows, three distinct mode types exist: a set of purely convected, solenoidal vortical disturbances; a set of irrotational potential disturbances, and a family of purely convected entropy disturbances. In nonuniform, nonaxial flows the three set of modes are coupled, and their characteristics change. The initial work of Kerrebrock [8] in this area has been extended more recently with the aid of different mathematical and numerical techniques by, among others, Golubev and Atassi [9,10], Tam and Ariault [11], Kousen [12], Cooper and Peake [13], Nijboer [14], and Atassi et al. [15].

Two families of solutions have been identified: a *nearly sonic* set, analogous to the acoustic modes in uniform flows, and a vorticity-dominated *nearly convected* set, analogous to the vortical and entropic waves in irrotational flows. The nearly sonic modes are pressure-dominated and have in general a small vortical component. Similarly, the nearly convected modes have a small pressure content, can be an infinite number, and also cluster toward the ends of a critical layer, corresponding to perfect convection.

The spectrum of acoustic-vorticity modes for an arbitrary background flow can be completed by a continuum of convected wave numbers corresponding to disturbances of a nonmodal type [16]. These disturbances are not taken into account in the present analysis, but it is worth pointing out that there may be situations in which both the convected and the nearly convected disturbances could contribute significantly to the unsteady pressure [16,17].

Wave-splitting methods have been extensively used in CFD boundary conditions to determine the direction in which information propagates and to prevent spurious reflections from the boundaries. When applied *inside* the computational domain, the technique lends itself to the extraction of noise information from the available CFD solutions [18].

Methods belonging to this class differ in the assumptions made regarding the mean flow and/or in the technique used to compute the pressure amplitudes once the eigenfunctions have been determined. Wilson [18] successfully applied a wave-splitting procedure to derive quantitative tone-noise information from steady and unsteady CFD solutions under the assumption of three-dimensional irrotational uniform axial flow in a hard-wall parallel annular duct. The method was devised to handle also vortical waves, but only for uniform axial flows for which an analytic Bessel–Fourier harmonic formulation exists. A modal decomposition of the flowfield as a noise postprocessing method was also proposed by Ovenden and Rienstra [19] for a homentropic potential flow in a slowly varying annular duct. The significant aspect of the latter method resides in the least-squares technique employed to calculate the modal amplitudes, and, for this reason, it will be reviewed and discussed in the next paragraph. Recently, Vilenski [20] extended the triple-plane pressure-matching method of Ovenden and Rienstra [19] to the case of swirling vortical flows.

The wave-splitting code used in the present study is based upon the eigenmode analysis of Moinier and Giles [21] which allows one to perform a normal mode analysis of nonuniform viscous or inviscid flows. The ability to handle nonuniform swirling flows constitutes a significant advantage over previous methods, and facilitates its application to real turbomachinery problems such as fan/OGV interaction. The identification method used to distinguish between pressure-dominated and vorticity-dominated modes used in the current analysis works very well for the classical problem of small-amplitude disturbances in an inviscid uniform axial flow, but also for several cases of ducted nonuniform swirling flows representative of turbomachinery applications as shown in [21,22].

Two different methods can be used to determine the unknown modal amplitudes: the left-right eigenvector method (L-R) and the triple-plane pressure-matching method (3P). The former approach exploits the orthogonality of the right and left eigenvectors of the generalized eigenvalue problem for the axial wave number to calculate the modal amplitudes, whereas the latter uses a triple-plane pressure-matching method for swirling vortical flows. The two methods are briefly outlined below.

1. L-R Method

Once the eigenvalues and the corresponding eigenvectors of the generalized eigenvalue problem for the axial wave number have been determined, the CFD solution can be reconstructed as the sum of the right eigenvectors in the form

$$\mathbf{H_m} = \sum_n A_{mn} \mathbf{u_n^R} \tag{3}$$

where $\mathbf{H_m}$ indicates the Fourier transform of the solution of order m, A_{mn} are the unknown modal amplitudes, and $\mathbf{u_n^R}$ are the right eigenvectors. The amplitudes A_{mn} can be determined by exploiting the orthogonality of left and right eigenvectors, as follows:

$$\mathbf{u_n^L} \cdot \mathbf{u_k^R} = \delta_{nk} \Rightarrow \mathbf{u_n^L} \cdot \mathbf{H_m} = A_{mn} \tag{4}$$

For a given frequency ω and circumferential mode number m and under the assumption of completeness, the acoustic field can then be expressed in terms of the eigenfunctions ψ_{mn} as

$$p(x, r, \theta, t) = \sum_n A_{mn}^{\pm} \psi_{mn}^{\pm}(x, r) e^{ik_{mn}^{\pm} x} e^{i\omega t + im\theta} \tag{5}$$

2. Triple-Plane Pressure-Matching Method

In the 3P method, the matching between the CFD solution and the wave-splitting flow model is done, as the name suggests, for a *single* variable: *pressure*. This choice accomplishes three main objectives:

1) The most physically significant flow variable in noise modeling, usually readily available, is considered.

2) The choice of a single variable removes any inconsistency at the interface.

3) The potentially harmful vortical contamination to which methods employing pressure and velocity are more sensitive is eliminated.

On the other hand, in order to distinguish between left and right traveling modes using a single variable, the number of matching planes must be greater than one. In the analysis of Ovenden and Rienstra [19], the matching zone is extended to three axial planes in an attempt to smooth out possible errors and make a better use of the information available. This choice leads to an overdetermined set of equations for the modal amplitudes that has to be solved via a least-squares fit.

Suppose that at the three axial planes x_0, x_1 and $x_2 (x_0 < x_1 < x_2)$, representing the matching zone, the Fourier component of the pressure, $P_{\omega m}(x)$, is known. Matching the modal expression in

Eq. (5) with the known pressure $P_{\omega m}(x)$ at the three axial planes leads to the overdetermined system below for the modal amplitudes:

$$\sum_n A^{\pm}_{mn}\psi^{\pm}_{mn}(x_0, r) = P_{\omega m}(x_0, r) \tag{6a}$$

$$\sum_n A^{\pm}_{mn}\psi^{\pm}_{mn}(x_1, r)e^{ik^{\pm}_{mn}(x_1-x_0)} = P_{\omega m}(x_1, r) \tag{6b}$$

$$\sum_n A^{\pm}_{mn}\psi^{\pm}_{mn}(x_2, r)e^{ik^{\pm}_{mn}(x_2-x_0)} = P_{\omega m}(x_2, r) \tag{6c}$$

The problem defined by Eq. (6) is solved via a least-squares approach to achieve the best fit using the LAPACK mathematical libraries.[¶]

The 3P method described above can be used with uniform axial and nonuniform swirling mean flows. The possibility of choosing the mean flow profile will allow a comparison between the L-R and 3P amplitude-calculation strategies, and it will enable one to isolate and quantify the effect of swirl and flow nonuniformity on the noise predictions.

For brevity, the methods will be denoted with the subscripts U and NU to indicate a uniform potential and a nonuniform swirling flow model, respectively. In other words, from now on, the wave-splitting methods will be referred to as $3P_U$, $3P_{NU}$, L-R_U, and L-R_{NU}.

III. Sound Power in Nonuniform Flows

To investigate the effects of a nonuniform swirling mean flow on the interaction tone-noise prediction, it is paramount to establish a meaningful (and, ideally, measurable) indicator. The quantity more commonly used to evaluate the noise emitted by rotor–stator interaction is the casing sound pressure level (SPL). This measure, although usually readily available in experiments, may not be ideal for instance to compare the acoustic benefits of different OGV designs, especially for nonuniform swirling flows typical of turbomachinery applications for reasons that will be explained in detail in Sec. IV.D. Therefore, it is important to quantify the amount of energy produced by a noise source in nonuniform swirling flows. Although in general the acoustic energy is not conserved in a nonuniform flow [23], Atassi [1] devised a simplified version of the first-order energy equation in the high-frequency limit for which the acoustic energy is locally conserved.

From the analysis presented in [1] it follows that in the high-frequency limit, typical of fan acoustics, the sound power can be calculated by integrating on an axial plane the mean flux of acoustic energy across it. The axial component of the energy flux vector can be expressed as

$$\mathbf{I}\cdot\mathbf{e}_x = I_x = (p' + \rho_0 u_x U_{0x} + \rho_0 u_\theta U_{0\theta})\left(u_x + \frac{\rho'}{\rho_0}U_{0x}\right) \tag{7}$$

and the average acoustic power is then given by $W = \iint_S \langle I_x\rangle \,\mathrm{d}S$. A normal mode analysis of the linearized Euler equations leads to the following modal expression for the sound power of a ducted nonuniform swirling mean flow:

$$\begin{aligned} W = \pi\Re\Bigg\{&\sum_{n=1}^{N_r}\sum_{n'=1}^{N_r}\sum_{m=1}^{N_\theta}\mathrm{sgn}(n)e^{i(k_{mn}-k_{mn'})x} \\ &\times\int_{r_h}^{r_t}\Big(P_{mn}X^*_{mn'} + \frac{U_{0x}}{\rho_0}P_{mn}R^*_{mn'} + \rho_0 U_{0x}X_{mn}X^*_{mn'} \\ &+ U^2_{0x}R_{mn}X^*_{mn'} + \rho_0 U_{0\theta}T_{mn}X^*_{mn'} + U_{0x}U_{0\theta}T_{mn}R^*_{mn'}\Big)r\,\mathrm{d}r\Bigg\} \end{aligned} \tag{8}$$

where N_r and N_θ denote the number of radial and circumferential propagating modes; $*$ indicates the complex conjugate; P_{mn}, X_{mn}, R_{mn}, and T_{mn} correspond to the eigenfunctions of pressure, axial velocity, density, and azimuthal velocity perturbations, respectively; $\mathrm{sgn}(n) = 1$ for downstream-propagating modes, and $\mathrm{sgn}(n) = -1$ for upstream-traveling modes.

A mode analysis of the linearized Euler or Navier–Stokes equations for a nonuniform swirling base flow leads to a non-Sturm–Liouville eigenvalue problem for the axial wave number, and the corresponding eigenfunctions are nonorthogonal. The nonorthogonality of the duct modes gives rise to interference effects between different radial modes and therefore induces a variation of the sound power with the axial coordinate x as a consequence of the different axial wave numbers. The effect of the interference terms on the modal sound power expression is clearly illustrated by the double summation over the radial mode indexes n and n', and by the exponential term in Eq. (8). For the sound power to be strictly conserved, the contribution due to the interference terms ($n \neq n'$) must equal zero.

In any real turbomachinery application, due to the mean flow vorticity and nonuniformity, the sound power is not strictly conserved. In practice, though, the acoustic power can be retained as locally conserved if the contributions of the interference terms amount to a negligible fraction of the total emitted sound power.

In the present study, the modal expression expressed by Eq. (8) has been adopted for all the wave-splitting methods using a nonuniform swirling background flow in the computation of the total sound power.

IV. Numerical Results

The range of applicability and accuracy of the postprocessing methods presented above are assessed using four examples of increasing geometric and flow complexity in which the effects of each of the methods' underlying assumptions are examined.

In real turbomachinery applications, the simplifying assumptions of annular cylindrical duct and uniform axial mean flow are violated to different degrees: the duct usually presents a varying cross section with a more pronounced area-change at the inlet of the bypass duct, and the flow is nonuniform with significant swirl, particularly upstream of the stators. It is therefore important to quantify the effects of these deviations from the ideal case on tone-noise extraction for each postprocessing method; this is what this paper sets out to do for discrete frequency tones generated by wake impingement for a series of numerical examples.

The first test case under consideration is the computational aeroacoustics (CAA) category 4 benchmark problem [24]: this test case investigates the impingement of a vortical gust on a cascade of unloaded flat plates in an inviscid uniform axial mean flow in an annular circular cylinder (Fig. 2). All the assumptions at the base of the postprocessing techniques are satisfied, and the outcome is expected to be virtually identical for each method, with only minor differences due to numerical errors. The aim of this test is to validate all the different methods for a well-documented benchmark problem with a known semi-analytical solution [25].

The second example aims at assessing the influence of moderate flow nonuniformity on the application and the accuracy of the postprocessing methods. The CAA benchmark problem is modified by the introduction of axial shear in the mean flow. None of the geometric parameters is changed, so that the flat plates remain

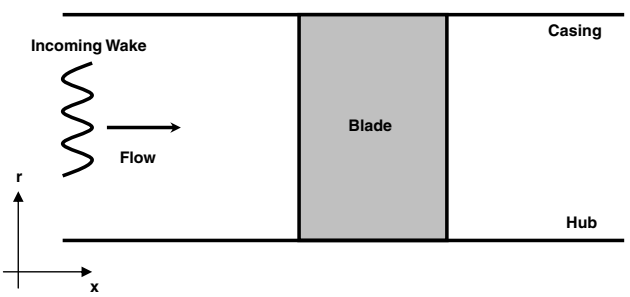

Fig. 2 Schematic of the interaction between an incoming vortical disturbance and a cascade of unloaded flat plates.

[¶]Data available online at http://www.netlib.org/lapack [retrieved 2008].

unloaded, and the inner and outer duct diameters remain constant for the entire axial extent of the computational domain. The degree of nonuniformity in the mean flow is also varied and the effects analyzed.

The third numerical example is again a simple modification of the CAA benchmark problem. In this case, the duct cross section is modified in the vane region with a rising hub line between the leading edge and the trailing edge of the flat plates. Upstream- and downstream of the vane the annulus inner and outer diameters are kept constant and no swirl is present. This example intends to test the flexibility and accuracy of the methods when the annular-duct assumption is violated in the source region, which could be an aspect of particular importance for the blade integration routine.

The last numerical example is a realistic fan/OGV configuration in which the cross section of the duct slowly varies along its entire length and the mean flow is nonuniform and nonaxial, with significant swirl upstream of the OGV leading edge.

As mentioned above, the modal sound power expression for nonuniform swirling flows in the high-frequency limit introduced in Sec. III will be used throughout. The extent to which the acoustic power can be retained as locally conserved in nonuniform, swirling flows, and the contributions of the cross terms and azimuthal velocity components will also be numerically assessed for the fan/OGV test case.

A. CAA Category 4 Benchmark Problem

The first example considered in the investigation of the postprocessing methods is the category 4 benchmark problem from the third CAA workshop on benchmark problems. The impingement of a vortical gust on an annular cascade of unloaded flat plates is examined for an inviscid uniform axial mean flow in a hard-wall annular circular cylinder. The duct hub-to-tip ratio is 0.5, the gap-to-chord ratio at the tip $2\pi r_T/(bV)$ is 1.0, and the mean flow axial Mach number is 0.5. The rotor blade tip Mach number, M_T, is 0.783, which leads to a fundamental chord-based reduced frequency of the incoming wake $\tilde{\omega} = \omega b/U = nB\Omega b/(a_0 M) = (2\pi B/V)(M_T/M) = 6.56$. No swirl is present and the flat plates are aligned with the axial mean flow hence unloaded.

The vortical gust is imposed at the inlet of the domain (Fig. 2) and is defined in cylindrical coordinates by the three perturbation velocity components:

$$u'_x = -\frac{U_{0x}^2}{\Omega r}\sum_{n=1}^{\infty} u_n e^{\mathrm{i}nB[\frac{\Omega}{U_{0x}}x+\theta+\phi(r)-\Omega t]}$$

$$u'_\theta = U_{0x}\sum_{n=1}^{\infty} u_n e^{\mathrm{i}nB[\frac{\Omega}{U_{0x}}x+\theta+\phi(r)-\Omega t]}, \qquad u'_r = 0 \tag{9}$$

where B is the number of rotor blades, Ω is the rotor rotational speed, U_{ox} is the axial mean flow speed, and V is the number of vanes. The integer n in Eq. (9) represents the harmonic index of the vortical excitation with upwash amplitude u_n. The gust defined above satisfies the solenoidal constraint for the vortical wake, and the phase shift along the span $\phi(r)$ is given by

$$\phi(r) = -2\pi\frac{q}{B}\frac{r - r_{\mathrm{in}}}{r_{\mathrm{out}} - r_{\mathrm{in}}} \tag{10}$$

where r_{in} is the duct inner radius and r_{out} is the outer radius. The number of phase changes along the span is determined by the integer q in Eq. (10). In the present analysis, the incoming vorticity is assumed radially in phase along the span, and 3-D nonreflecting boundary conditions are used at the inflow and outflow boundaries [22,26].

A good agreement between the numerical results obtained with the linearized CFD approach used in this study, and those obtained with a lifting surface model was previously reported in [22,27], and the same mesh resolution is used here. A time-linearized Euler finite volume method is employed to calculate the unsteady interaction on a uniform rectangular mesh with 113 points in the axial direction, 33 in the azimuthal direction and 65 radially. The test problem is a simple representation of the rotor–stator-interaction noise-generation mechanism for a blade-to-vane ratio of 16:24 (2:3). Only the first harmonic of the blade passing frequency (BPF) with $n = 1$ and $u_n = 0.1$ is analyzed here, and an interblade phase angle of -240 deg is applied at the periodic boundaries.

The analysis concentrates solely on cuton modes and the results in terms of casing SPL and sound power level (PWL) are summarized in Tables 1 and 2 for the first and second upstream- and downstream-propagating radial harmonics, respectively, for the only cuton circumferential mode $m = -8$. The values of the casing SPL and PWL in Tables 1 and 2 are averaged over the axial distance between the inlet and half-chord upstream of the leading edge for forward propagating noise and between half-chord downstream of the trailing edge and the outflow boundary for downstream-traveling sound waves.

The small values of the standard deviation of the axial variation, σ^2, calculated for the casing SPL and PWL, and reported in Tables 1 and 2, highlight the fact that the cuton waves propagate with unattenuated amplitudes away from the source, and how PWL is conserved. This demonstrates the validity of the calculation approach and enables us to compare the methods on average values of SPL and PWL, greatly simplifying the exposition of the results.

As expected, all the numerical techniques employed to extract tone-noise information from the converged CFD solution provide almost identical results. In fact, in the current example, none of the underlying assumptions is violated as the duct is an annular circular cylinder and the mean flow is inviscid, uniform and axial. The results obtained with a lifting surface model [25] are also included in Tables 1 and 2 as a further term of comparison. A good agreement between the numerical results obtained with a linearized CFD approach and those obtained with a lifting surface method were found, as previously reported by Wilson [27], who investigated the applicability of a time-linearized approach with analytically exact nonreflecting boundary conditions for uniform axial mean flow. This proves the validity of the calculation approach of all the postprocessing methods under investigation when their theoretical assumptions are exactly satisfied.

The performance of the wave-splitting methods can also be assessed by examining how well the unsteady pressure profile, P_m, for $m = -8$, obtained by a circumferential Fourier transform of the unsteady flowfield $p(x_0) = \Sigma_m P_m(x_0, r)e^{-im\theta_0}$, where $P_m(x_0, r) = \Sigma_n P_{mn}(x_0, r)e^{-ikx_0}$ is reconstructed as a sum of the eigenfunctions at a specified axial plane x_0. Figure 3a illustrates the comparison between the CFD data and the reconstructed real part of the

Table 1 Modal amplitudes of cuton upstream-propagating modes for the CAA category 4 benchmark problem ($m = -8$).

	AA		L-R_U		3P_U		Lifting surface
μ	dB	σ^2	dB	σ^2	dB	σ^2	dB
				SPL			
1	150.79	0.0	150.68	0.055	150.75	0.048	150.97
2	150.97	0.0	151.26	0.056	151.37	0.041	151.88
				PWL			
1	136.32	0.0	136.19	0.055	136.26	0.048	N/A
2	138.06	0.0	138.32	0.056	138.43	0.041	N/A

Table 2 Modal amplitudes of cuton downstream-propagating modes for the CAA category 4 benchmark problem ($m = -8$)

	AA		L-R_U		3P_U		Lifting surface
μ	dB	σ^2	dB	σ^2	dB	σ^2	dB
				SPL			
1	153.37	0.0	153.30	0.045	153.24	0.049	153.08
2	151.07	0.0	151.10	0.034	151.11	0.017	151.31
				PWL			
1	145.71	0.0	145.60	0.045	145.55	0.049	N/A
2	140.80	0.0	140.76	0.034	140.78	0.017	N/A

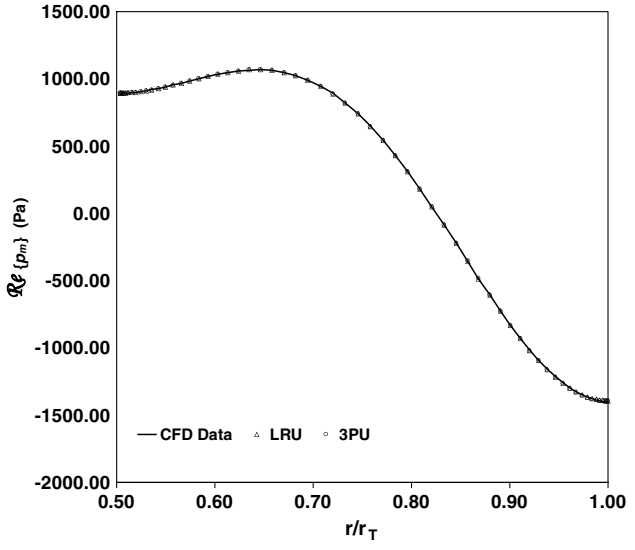

a)

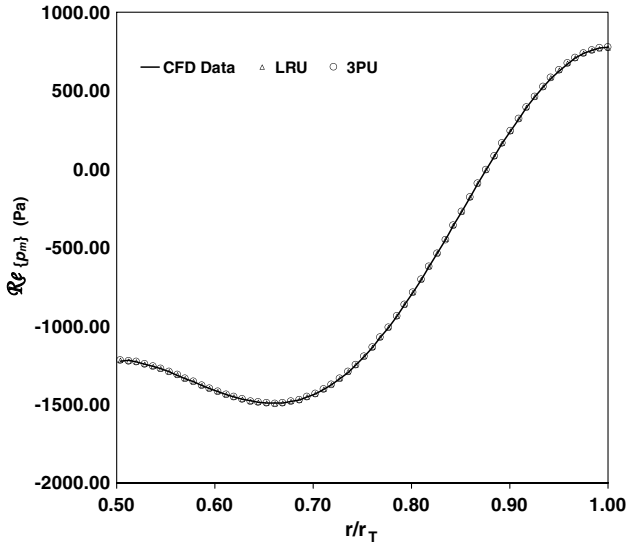

b)

Fig. 3 Comparison between the reconstructed unsteady pressure profile (real part) a) upstream and b) downstream of the flat plates and the circumferentially Fourier transform of the CFD data ($m = -8$).

amplitude of the unsteady pressure profile, $Re\{P_m\}$, at an axial plane upstream of the flat plate, and Fig. 3b for a plane downstream of the flat plates. For all the methods the agreement is excellent and the real part of the unsteady pressure perturbation amplitude is accurately reconstructed by including in the analysis only the first three cutoff radial modes.

In all the wave-splitting techniques' results, the same number of cutoff modes is included in the analysis. The influence of the number of decaying modes on the results is negligible, but it was nonetheless fixed for consistency. Sensitivity studies on the number and distribution of the radial points in which the eigenvalue problem is discretized and on the number and spacing between the axial planes have been conducted. No significant differences were observed for any of the wave-splitting methods, and the results are omitted for brevity.

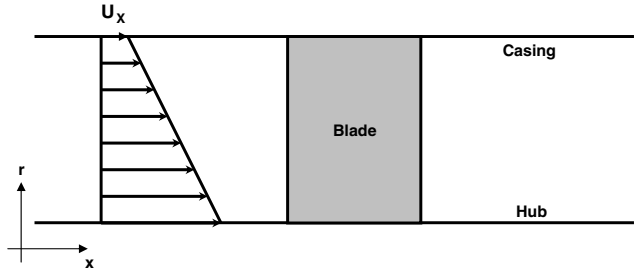

Fig. 4 Schematic illustration of the CAA category 4 benchmark problem with an axially sheared mean flow.

B. Axially Sheared Mean Flow

The CAA category 4 benchmark problem is modified to test the effects of mean flow nonuniformity on the postprocessing methods (see the schematic in Fig. 4). The mean axial shear distribution in Eq. (11) is superimposed to the otherwise uniform background flow U_{0x}, giving the axial velocity distribution in Eq. (12):

$$U_{x,\text{shear}}(r) = \frac{U_{0x}}{10}\left(1 - \frac{r}{r_T}\right)^{1/n} \tag{11}$$

$$U_x(r) = U_{0x} + U_{x,\text{shear}}(r) \tag{12}$$

The flat plates are still aligned to the axial mean flow and hence unloaded. The nonuniformity of the flow and the absence of swirl can be retained as an idealization of the mean flow behind a bypass guide vane, whose duty is to turn the flow to the axial direction. In this light, this represents an interesting preliminary test for the postprocessing methods in extracting near-field downstream-propagating noise information. At first, the exponent of the axial shear term, n, was set to 7.

A solenoidal vortical gust is imposed at the inlet of the domain, and the tone noise generated by the scattering of the impinging gust is quantified downstream of the flat-plate cascade in terms of casing SPL and PWL.

Table 3 summarizes the results obtained with the wave-splitting and the unsteady pressure integration techniques. The results are all very similar and the effect of the flow nonuniformity is negligible. Both the acoustic analogy (AA) approach and the wave-splitting methods based on a uniform axial flow seem to be able to cope with a moderate nonuniformity.

All the wave-splitting methods are able to reconstruct the unsteady pressure amplitude profile successfully; an example is shown in Fig. 5 for the real part of the unsteady pressure amplitude upstream of the flat plates.

The level of nonuniformity is dictated by the exponent n in the axial shear term in Eq. (11). A study was conducted on the effect of

Table 3 Modal amplitudes of cuton downstream-propagating modes for the CAA category 4 benchmark problem with axially sheared mean flow

	AA		$L\text{-}R_U$		$L\text{-}R_{NU}$		$3P_U$		$3P_{NU}$	
μ	dB	σ^2	dB	σ^2	dB	σ^2	dB	σ^2	dB	σ^2
					SPL					
1	155.10	0.0	155.07	0.022	155.09	0.019	155.05	0.019	155.08	0.023
2	150.70	0.0	150.63	0.153	150.61	0.046	150.59	0.035	150.58	0.019
					PWL					
1	147.58	0.0	147.52	0.022	147.51	0.019	147.51	0.019	147.50	0.023
2	141.40	0.0	141.31	0.153	141.35	0.046	141.27	0.035	141.32	0.019

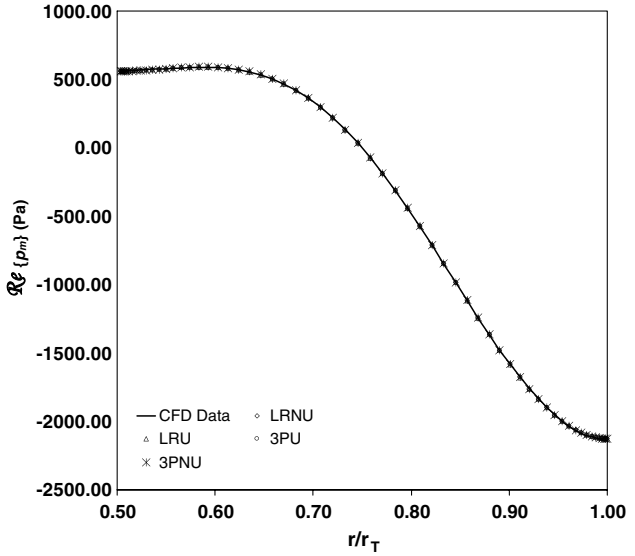

Fig. 5 Comparison between the reconstructed unsteady pressure profile (real part) upstream of the flat plates and the circumferentially Fourier transform of the CFD data for axially sheared flow ($m = -8$).

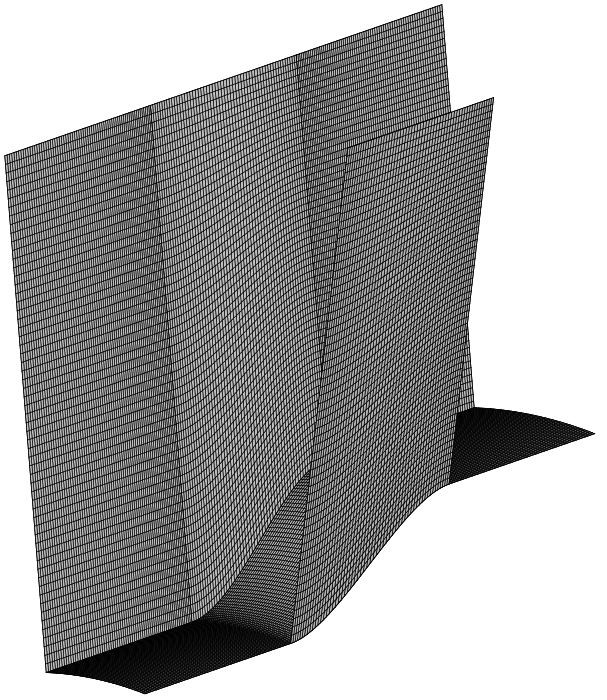

Fig. 6 Geometry and computational mesh (113 × 33 × 61) for the modified CAA category 4 benchmark test case with a varying duct hub line.

the radial distribution of axial shear by varying the n from 1 to 7, and no appreciable differences were observed between the various postprocessing methods. Both AA and the wave-splitting methods showed virtually no dependence on the nonuniformity of the mean flow examined here. The results in Table 3 support the conclusion reached in the previous Section, that in the absence of a strong nonuniformity or swirl, the uniform axial approximation of the mean flow is reasonable and acceptable.

C. Varying Duct

Modern high-bypass-ratio engines have a nonuniform bypass duct, particularly in the region leading up to the bypass stators, and in the vane passage. The variation in the duct cross section can affect the aerodynamic interaction mechanism between the fan wakes and the stator vanes through the changes to the mean flow in the vane passage and can modify the duct acoustic modes upstream- and downstream of the blade row. When the change in the cross-sectional area is located in the source region, methods based on the Ffowcs Williams–Hawkings model can be subject to significant errors due to the incorrect pressures integration and the ambiguous construction of the duct modes. In this respect, wave-splitting methods are more flexible as they are usually applied far away from the source in areas in which the duct can be considered locally straight.

To illustrate this point, the present analysis considers a simple variation to the standard CAA benchmark problem in which the duct hub line is defined by the following algebraic expression:

$$\begin{cases} r = r_{\text{in},1}, & x \le b/2 \\ r = r_{\text{in},1} + 3(r_{\text{in},2} - r_{\text{in},1})\left(\frac{x}{b/2} - 1\right)^2 - 2(r_{\text{in},2} - r_{\text{in},1})\left(\frac{x}{b/2} - 1\right)^3, & b/2 < x < b \\ r = r_{\text{in},2}, & x \ge b \end{cases} \tag{13}$$

In Eq. (13), $r_{\text{in},1}$ and $r_{\text{in},2}$ represent the values of the inner duct radius at the inflow and outflow, respectively, x is the axial coordinate and b is the chord of the flat plates, which are located between $x = b/2$ and $x = b$. The new duct geometry with the corresponding computational mesh is shown in Fig. 6.

This test case (originally used to illustrate the potential acoustic benefit attainable by mean flow acceleration [28]) represents a simple example apt to show the importance of the constant duct assumption in relating the unsteady pressure on the vanes with the pressure inside the duct in an acoustic analogy formulation.

The inner radius was chosen so that the hub-to-tip ratio varies from 0.5 at the inflow to 0.6 at the outflow. The exit Mach number is fixed at 0.5 at the exit of the domain. The computational mesh used has 113 points in the axial direction, 33 circumferentially and 61 radially (see Fig. 6). The walls are adiabatic and inviscid, and the flow is axial.

The application of the acoustic integration method to this test case could result in significant inaccuracies not just for its use of Green's functions for uniform flows, but mainly because of the necessity to conform to the circular-annular-duct assumption in the model. Important contributions of the unsteady pressures near the hub line might not be integrated correctly in an *equivalent* annular-duct model, giving rise to significant changes in the predicted noise levels. Figure 7 illustrates three possible equivalent ducts to integrate the vanes unsteady pressures and determine the radiated noise in terms of uniform-flow duct modes.

The variations of PWL for the different hub lines are summarized in Fig. 8 for downstream-propagating noise, and in Fig. 9 for upstream-propagating noise. Let us consider downstream-propagating noise first.

For downstream-propagating noise, a large variation of the PWL with the hub radius can be observed. Figure 8 shows that the second radial harmonic is predominantly responsible for such variation, whereas the first radial harmonic is less sensitive to the assumed duct inner radius. This may suggest that for the first radial mode the contribution of the unsteady pressures in the lower part of the vanes is not significant when integrated over the vane surface, and that the small changes observed in the PWL for this radial harmonic are due

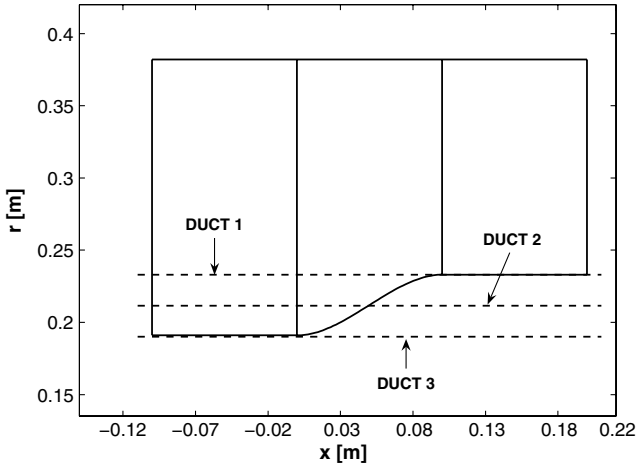

Fig. 7 Three possible straight ducts to be used in an acoustic analogy approach (AA) for the modified CAA category 4 benchmark test case with a varying duct hub line.

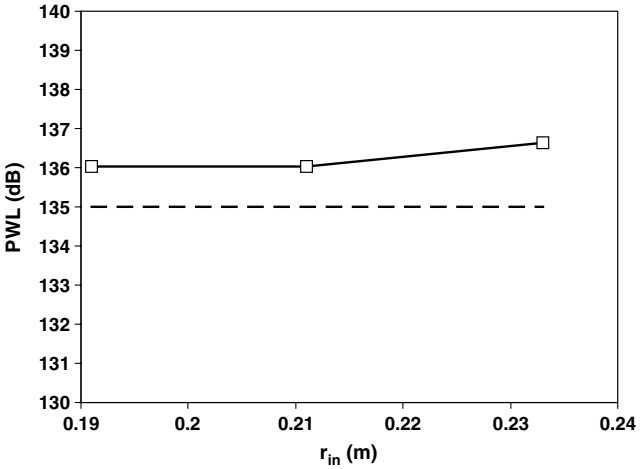

Fig. 9 Variation of the predicted PWL (AA) with the inner radius for the upstream-propagating mode (CAA category 4 with varying hub line). The dashed line represents the predicted value obtained with the wave-splitting methods.

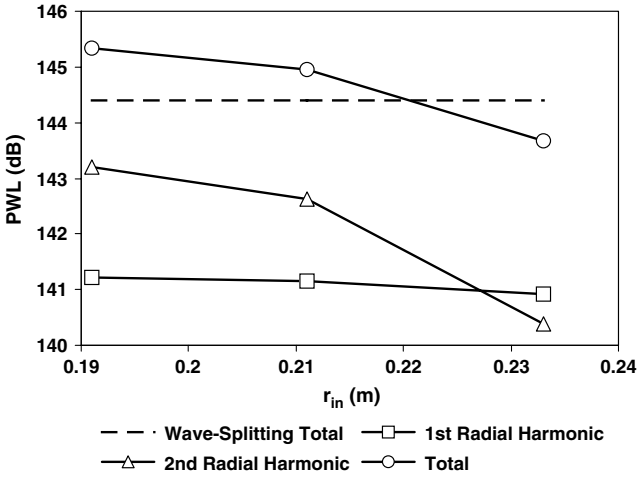

Fig. 8 Variation of the predicted PWL (AA) with the inner radius for downstream-propagating modes (CAA category 4 with varying hub line). The dashed line represents the predicted value obtained with the wave-splitting methods.

to the duct variation effects on the duct modes, i.e., a change in the hub-to-tip ratio slightly changes the cuton ratio of the mode. The shape of the first duct radial mode, which is typically tip-dominated, can intuitively explain this consideration.

For the second radial mode the cancellation of the different unsteady pressure fields at different spanwise locations is much more involved. Two extreme situations are considered for the duct inner radius, corresponding to duct 1 and duct 3 in Fig. 7, respectively.

In the first case, the duct is taken to coincide with the real duct downstream of the flat plates. As a consequence of this, the duct modes considered in the modal expression of the Green function are correct (ignoring the flow nonuniformity), but the unsteady pressure integration results limited to part of the vane surface, exposing the method to potential nonnegligible errors. In this case, the contribution of the vane unsteady pressures in Eq. (2) near the hub is lost, resulting in a underestimation of the downstream noise.

In the second case, the annulus is taken to coincide with the inlet duct so as to include all the pressures contributions in the integration. On the other hand, this choice implies that the unsteady pressures amplitudes are expressed in terms of fictitious duct modes that bear little relation with the actual duct downstream of the noise source. When the integration is extended to the entire vane surface, the second radial harmonic becomes more cuton and artificially noisier. An intermediate case is also considered in Fig. 8 (see duct 2 in Fig. 7), highlighting the tradeoff between a correct pressure integration and a correct modal expression for the Green function, to which the second radial harmonic is more sensitive.

Similar considerations can be carried out for upstream-propagating noise. In this case only one radial harmonic is cuton and the duct is taken to coincide with the actual duct upstream of the flat plates. For upstream-propagating noise there is no conflict between the unsteady pressure integration and the duct modes, but the predicted PWL is about 1 dB higher than the corresponding values extracted with a wave-splitting method. This may relate to the details of the integration of the unsteady pressures on the vane surface. Unfortunately, it was not possible to investigate this issue further.

The results presented thus far suggest that the use of an acoustic integration method for fan/OGV interaction tone noise is more limited by the erroneous integration of the unsteady pressures on the vane surface due to the assumed duct geometry than by the flow nonuniformity. This is particularly true for downstream-propagating noise due to the relatively uniform mean flow downstream of the OGV.

The tradeoff between a correct pressure integration and an appropriate modal expression for the Green function can be a limiting factor in the application of an AA method to a real fan/OGV configuration, particularly if one wishes to assess the acoustic benefits of a new vane design over a datum one. In such a situation, a certain region of the vane could contribute significantly for one geometry and not for the other, leading to an incorrect ranking of the designs. Therefore, a preliminary study of the variation of the predicted noise levels due to the duct approximation should always be carried out to quantify the errors and the sensitivity of the results.

Another possible issue to bear in mind regard the actual integration process on a surface that varies within the assumed equivalent duct. This aspect requires further study.

Table 4 Modal amplitudes of cuton downstream-propagating modes for the CAA category 4 benchmark problem with rising hub line

	$L\text{-}R_U$		$L\text{-}R_{NU}$		$3P_U$		$3P_{NU}$	
μ	dB	σ^2	dB	σ^2	dB	σ^2	dB	σ^2
				SPL				
1	149.49	0.029	149.55	0.037	149.51	0.061	149.56	0.034
2	153.16	0.097	153.14	0.096	153.09	0.104	153.09	0.105
Sum	154.71	——	154.72	——	154.67	——	154.69	——
				PWL				
1	141.33	0.027	141.33	0.036	141.34	0.060	141.35	0.049
2	141.44	0.091	141.56	0.088	141.37	0.102	141.46	0.039
Sum	144.42	——	144.45	——	144.36	——	144.41	——

Table 5 Modal amplitudes of cuton upstream-propagating modes for the CAA category 4 benchmark problem with rising hub line

		L-R_U		L-R_{NU}		3P_U		3P_{NU}	
	μ	dB	σ^2	dB	σ^2	dB	σ^2	dB	σ^2
SPL	1	148.29	0.111	148.47	0.102	148.43	0.111	148.49	0.069
PWL	1	134.94	0.109	134.69	0.020	135.04	0.109	134.67	0.028

The results for downstream- and upstream-propagating noise, obtained by analyzing the CFD solution with the wave-splitting methods, are summarized in Tables 4 and 5, respectively. No significant differences are found between the methods, suggesting that moderate flow nonuniformity does not affect the predicted noise levels, in either directions, i.e., upstream- and downstream-propagating.

All the wave-splitting methods are able to accurately reconstruct the real part of the unsteady pressure amplitude as a sum of the eigenmodes at axial stations located both downstream- and upstream of the flat plates.

D. Fan/OGV Test Case

The postprocessing techniques investigated thus far are applied to a realistic fan/OGV configuration. The stage under consideration comprises 26 rotor blades and 58 straight stator vanes. A meridional view of the stage is depicted in Fig. 10. The discrete frequency interaction tones generated by the impingement of the fan wakes on the bypass OGV are investigated at a speed representative of cutback operation at twice the blade passing frequency (2BPF) using a linearized CFD approach. The calculation methodology entails a stage-steady calculation to derive the OGV mean flow and the fan wake harmonic by circumferentially Fourier-decomposing the rotor solution. The second harmonic of the rotor wake is then imposed at the inlet of the stator domain (immediately upstream of the vane leading edge) in the single passage, with uncoupled linear unsteady OGV calculation used to investigate the wake/vane interaction noise generation. All the postprocessing methods are used to extract near-field noise information from the linear solution for upstream as well as downstream-propagating modes.

The OGV computational domain extends from station 3 in Fig. 10 to station 4, covering approximately four stator axial chords. The computational grid has a H-O-H topology with a body-fitted O-mesh around the vane, and the domain was discretized with 2.2 million nodes (per vane passage) with approximately 200 points around the vane sections, 60 in the circumferential direction, and 101 radially. Three-dimensional nonreflecting boundary conditions are applied at the inlet and exit boundaries, and the phase difference experienced by neighboring vanes is incorporated in the interblade phase angle at the periodic boundaries. The postprocessing methods are applied to extract near-field noise information propagating upstream as well as downstream of the OGV.

At the prescribed reduced frequency, based on half the stator chord, $\tilde{\omega} = c_s\omega/2U \sim 6.0$, one spinning mode with circumferential mode number $m = -6$ propagates unattenuated upstream as well as downstream of the bypass OGV; an additional circumferential mode with circumferential mode order $m = 52$ propagates with constant amplitude only in the downstream direction.

The spinning mode $m = 52$ does not propagate upstream due to the significant swirl ahead of the OGV leading edge. This is clearly illustrated in Fig. 11, in which the eigenvalues' spectrum upstream of the bypass stator for the mode $m = 52$ is presented for an idealized uniform axial mean flow, and for the actual nonuniform background flow. In the latter case, the nonuniformity and swirl are such to prevent this corotating mode from propagating, as it would otherwise

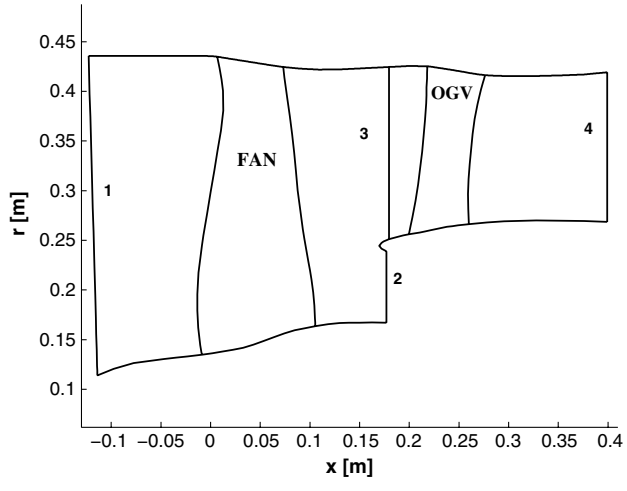

Fig. 10 Outline of the fan stage.

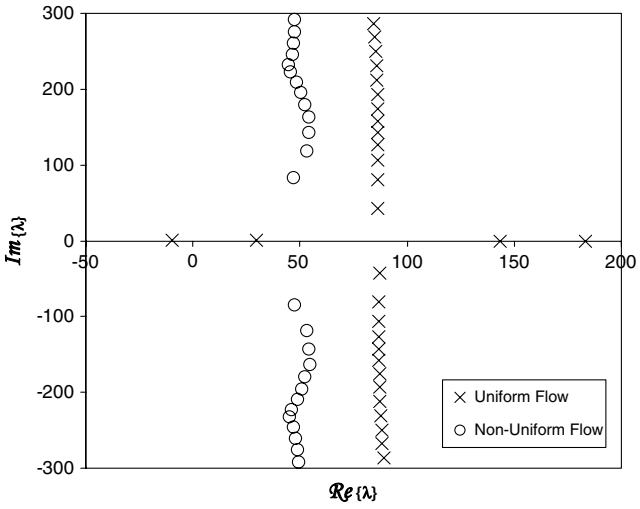

Fig. 11 Eigenvalues' spectrum upstream of the OGV for the circumferential mode $m = 52$.

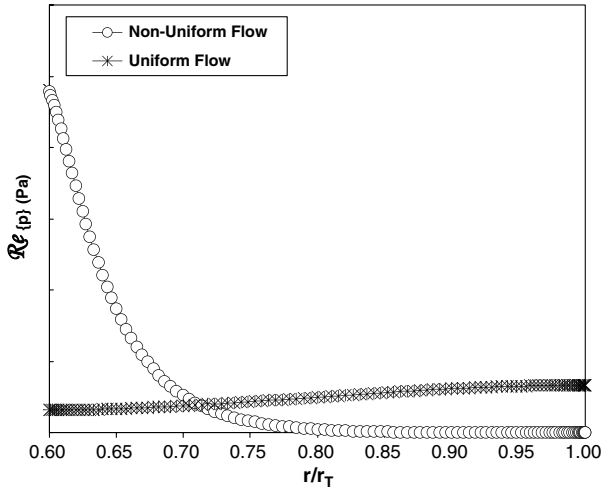

Fig. 12 First upstream-propagating radial harmonic for the circumferential mode $m = -6$ for a uniform axial and a nonuniform swirling flow.

Table 6 Variation of PWL modal amplitudes of cuton downstream-propagating modes for the circumferential modes $m = -6$ and 52 for $\Delta\text{PWL} = \text{PWL}_{\text{L-RNU}}\text{-PWL}$

	L-R_U		L-R_{NU}		$3P_U$		$3P_{NU}$	
μ	dB	σ^2	dB	σ^2	dB	σ^2	dB	σ^2
				$m = -6$				
Total	0.05	0.03	0.0	0.03	0.05	0.03	0.02	0.03
				$m = 52$				
Total	0.30	0.04	0.0	0.03	0.38	0.04	0.07	0.03

do in the absence of swirl. Figure 11 shows how the two cuton uniform-flow radial modes become cutoff modes when the actual nonuniform swirling flow profile is considered.

In addition, the mean flow nonuniformity and swirl can substantially modify the shape of the eigenfunctions, transforming, for instance, a typically tip-dominated radial mode into a hub-dominated one. This aspect can have important consequences if, as common practice, the propagating noise is quantified in terms of the casing SPL, the quantity more commonly available from experiments, rather than in terms of sound power (PWL). A typical example is represented by the first radial harmonic of mode $m = -6$ at 2BPF at cutback. For this mode and at this operating condition, the pressure eigenfunctions calculated upstream of the OGV differ substantially in the case of uniform axial and nonuniform swirling flows [13]. Figure 12 shows how the shape of the first radial mode changes with swirl, shifting from a casing-dominated function to a hub-dominated one.

If the acoustic benefits of one OGV design against a datum vane are assessed in terms of casing SPL when the corresponding pressure eigenfunctions are different, misleading results could be obtained. This represents an issue of particular importance in those cases in which the flow is strongly nonuniform and/or is characterized by a significant swirl velocity component. Incidentally, the shape of the eigenfunctions in the presence of swirl may be important in determining the most suitable location of acoustic liners. Downstream of the OGV, due to the modest amount of swirl, the shapes of the pressure eigenfunctions do not (usually) change significantly, and a *quantitative* acoustic benefit assessment can still be carried out in terms of SPL values (with the appropriate precautions).

In view of the above considerations, the comparison between the various tone-noise postprocessing methods will be evaluated only in terms of PWL, and the high-frequency modal expression discussed in Sec. III will be adopted for those methods taking into consideration the actual nonuniform swirling mean flow.

In a realistic fan stage, the mean flow upstream of the OGV is highly nonuniform with a strong swirl component, and the bypass duct cross section is slowly varying from the inlet to the exit of the computational domain as shown in Fig. 12. These aspects violate the main geometric and mean flow assumptions of the L-R_U, $3P_U$ and AA methods, therefore the impact of such conditions on the predicted noise will be assessed against the L-R_{NU} and $3P_{NU}$ methods.

1. *Downstream Propagating Noise*

The results obtained for downstream-propagating noise are presented first. Figures 13a and 13b show the modal decomposition of the PWL predicted by all the methods for the propagating modes $m = -6$ and 52, respectively. The PWL values are obtained as an average of the values at ten axial positions between approximately half-chord downstream of the vane trailing edge and the outflow boundary.

The modal decomposition in Fig. 13b for $m = 52$ shows differences of the order of a few tenths of dB between the radial modes' contributions predicted by the wave-splitting methods employing either a uniform or a nonuniform flow model. These differences do not cancel out, and an overall difference of $\sim$0.4 dB in the total PWL is found (see Table 6). This result is in line with the observation that a uniform approximation might be a reasonable

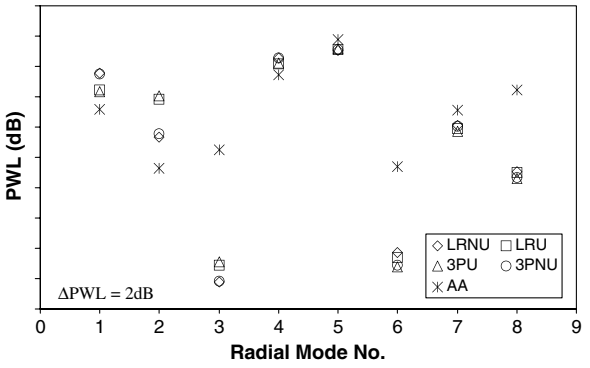

a)

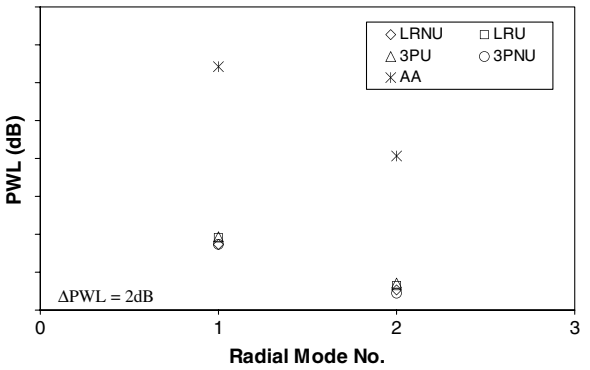

b)

Fig. 13 PWL modal decomposition for downstream-propagating noise at 2BPF at cutback for the spinning mode a) $m = -6$ and b) $m = 52$.

approximation for the flowfield downstream of the bypass stators, although in many situations a delta of 0.4 dB may not be acceptable. A comparison between the PWL results, calculated as the sum of the radial modes, obtained with the L-R and the 3P methods for uniform and nonuniform mean flows allows to isolate and quantify the effect of the nonuniform swirling mean flow in $\sim$0.4 dB for $m = 52$, and in less than 0.1 dB for the mode $m = -6$. In this case, the almost uniform nature of the flow in the bypass duct (downstream of the OGV) allows one to use uniform implementations of the wave-splitting technique with reasonably accurate results.

Upon a closer examination of Fig. 13a, differences of up to 2 dB are observed for some radial modes for $m = -6$ between methods employing uniform and nonuniform flows. Although these differences balance out when a sum is calculated, leading to a negligible difference between the predicted values of the total sound power (see Table 6), it is still advisable to include the actual nonuniform swirling flow profile in the treatment when possible.

The results obtained with the AA method for an equivalent duct extending from the minimum to the maximum values of the radial coordinate are shown in Fig. 13 for illustrative purposes only. Nevertheless, it is interesting to observe, particularly for $m = 52$, that the PWL of the two radial harmonics are significantly overpredicted. This may hint at a problem concerning radial modes with a cuton

Table 7 Symbols convention used to identify each term appearing in Eq. (8)

Symbol	Modal term
◇	$P_{mn}X^*_{mn'}$
△	$(U_{0x}/\rho_0)P_{mn}R^*_{mn'}$
□	$\rho_0 U_{ox}X_{mn}X^*_{mn'}$
*	$U^2_{0x}R_{mn}X^*_{mn'}$
○	$\rho_0 U_{0\theta}T_{mn}X^*_{mn'}$
+	$\rho_0 U_{0\theta}T_{mn}R^*_{mn'}$

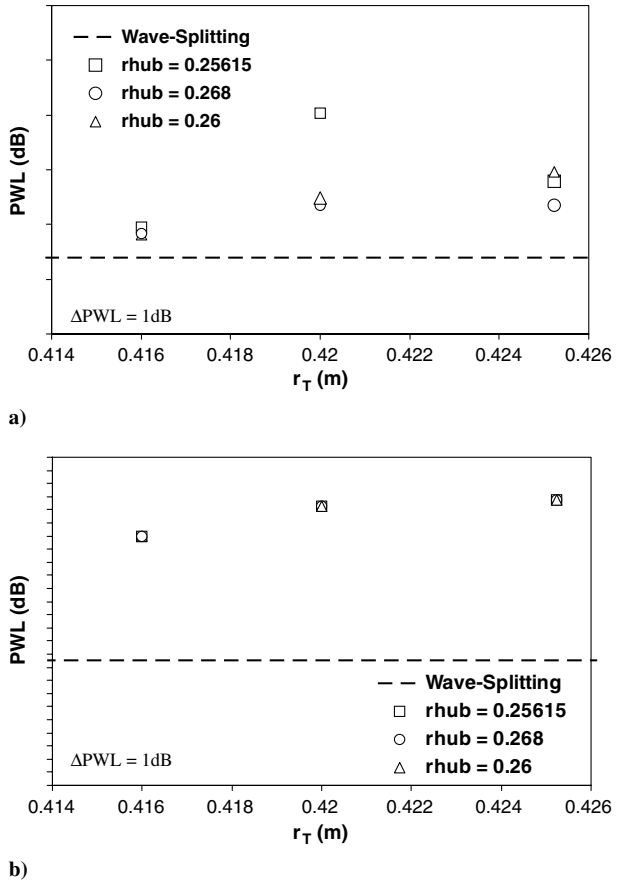

Fig. 14 Variation of the predicted PWL (AA) with the inner radius for downstream-propagating modes for a) $m = -6$ and b) $m = 52$ at 2BPF at cutback.

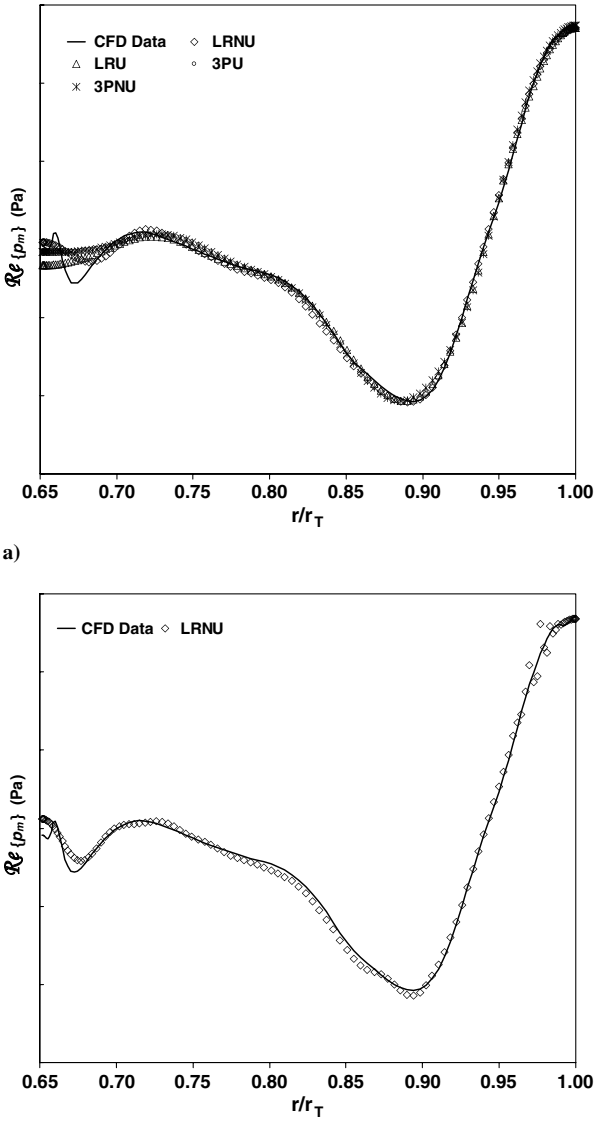

Fig. 15 Comparison between the reconstructed unsteady pressure profile (real part) downstream of the OGV and the circumferentially Fourier transform of the CFD data for the spinning mode $m = 52$: a) the first 15 radial modes are used in the sum and b) the number of radial modes is increased to 25.

ratio very close to 1, as is the case for both radial modes at $m = 52$. A similar issue can be found for the last radial mode at $m = -6$ which is very close to being cutoff.

The PWL values predicted using the acoustic analogy approach (AA) are shown in Fig. 14. As previously observed, the integration routine method is sensitive to the assumed straight duct when the real duct cross section varies in the vane region. The variation in the predicted downstream PWL with inner and outer radii for mode $m = -6$ is shown in Fig. 14a. In this case, it is apparent how the dependency upon the choice of an equivalent duct is strong, even for plausible diameters values and small radius changes.

For mode $m = -6$ the predicted noise varies with both the inner and outer radii, as one could intuitively expect by looking at the PWL modal decomposition in Fig. 13a. The three major contributions come from the first, fourth and fifth radial harmonics and a strong dependency upon the integration area is to be expected.

On the other hand, for mode $m = 52$ the PWL values depend almost entirely on the outer diameter as illustrated in Fig. 14b. This is probably due to the fact that of the two cuton radial harmonics, the dominant one is the first, which is casing-dominated, and the integral effect of the unsteady pressure near the hub has a negligible impact on the overall level of the downstream-propagating noise.

When the results obtained with AA are compared with the values of PWL predicted with a wave-splitting method, a large difference is found. As pointed out earlier, such discrepancy is believed to be the result of the overprediction of the pressure amplitudes for modes very near cutoff, in this particular case, both radial modes at $m = 52$ and the last radial mode at $m = -6$.

To corroborate the accuracy of the wave-splitting methods, the real part of the unsteady pressure for the circumferential mode $m = 52$ is reconstructed as a sum of the computed eigenfunctions, as shown in Fig. 15a (similar results were found for the mode $m = -6$, but are omitted here for brevity). The axial plane under consideration is one chord downstream of the OGV trailing edge. A small discrepancy in the matching is noticeable near the hub even when the nonuniform flow profile is taken into account. This is probably due to the large number of radial harmonics required for an accurate reconstruction near the inner radius. As a matter of fact, the matching can be improved by increasing the number of radial eigenfunctions in the sum, as shown in Fig. 15b for the L-R method. In this case the summation was extended from 15 to 25 radial harmonics. Although the inclusion of a larger number of modes improves the reconstruction of the pressure profile, the overall noise prediction does not change appreciably. Also, for a nonuniform swirling flow, the mode identification process can become extremely complicated when very large numbers of radial harmonics need to be taken into consideration as nearly convected modes, with a nonzero associated pressure field, can erroneously be sorted as acoustic. Furthermore, it is paramount to consider that the number of modes that can be accurately resolved is limited by the mesh resolution. In general, a good agreement is found between the reconstructed real part of the unsteady pressure and the Fourier transform of the CFD data, confirming the accuracy of the wave-splitting techniques under investigation.

A last remark must be made regarding the contribution of mean swirl and nonuniformity in the computed sound power, and the level of approximation incurred in considering the flow behind the bypass OGV axial and uniform. To this end, it is paramount to examine the contributions of each of the terms in Eq. (8). The most effective and clear way of presenting the results is to adopt the same representation style of [1].

For a given frequency and circumferential mode number, m, each of the cuton radial modes is plotted separately and is identified by its radial index n. The interference contributions are illustrated by plotting the sound power of each term in Eq. (8) for a given radial mode of index n, against the corresponding items of radial mode index $n' \neq n$.

Throughout this work different symbols are used to denote each term appearing in Eq. (8). The diamond (◇), triangle (△), square (□), and star (*) correspond to the first four terms, respectively. The open circle (○) and the cross (+) symbols correspond to the fifth and sixth terms, which contain the mean flow swirl velocity. This convention is summarized in Table 7.

For the circumferential mode $m = -6$ at 2BPF cutback, Fig. 16 shows the results for just six of the nine propagating radial harmonics; a reduced number of modes is presented for sake of clarity and without any critical loss of information. It is apparent that the contribution due to the interference terms is negligible compared with the noninterference term ($n' = n$) for every radial mode. In the noninterference terms, the dominant contribution is generally due to the first three terms, and the terms directly depending on the mean swirl (i.e., the fifth and sixth terms) are very small, as one might expect, due to the relatively small amount of swirl downstream of the OGV (see Fig. 17). Similar results were also found for the circumferential mode $m = 52$, and they seem to suggest that neglecting the terms related to the mean swirl in the modal expression of the sound power would produce small differences.

The results illustrated in Fig. 16 indicate that even in a nonuniform swirling flow with nonzero mean vorticity, the sound power is conserved over a distance of the order of the characteristics acoustic wavelength. To demonstrate this point further, the calculated acoustic sound power for the spinning modes $m = -6$ and 52 at

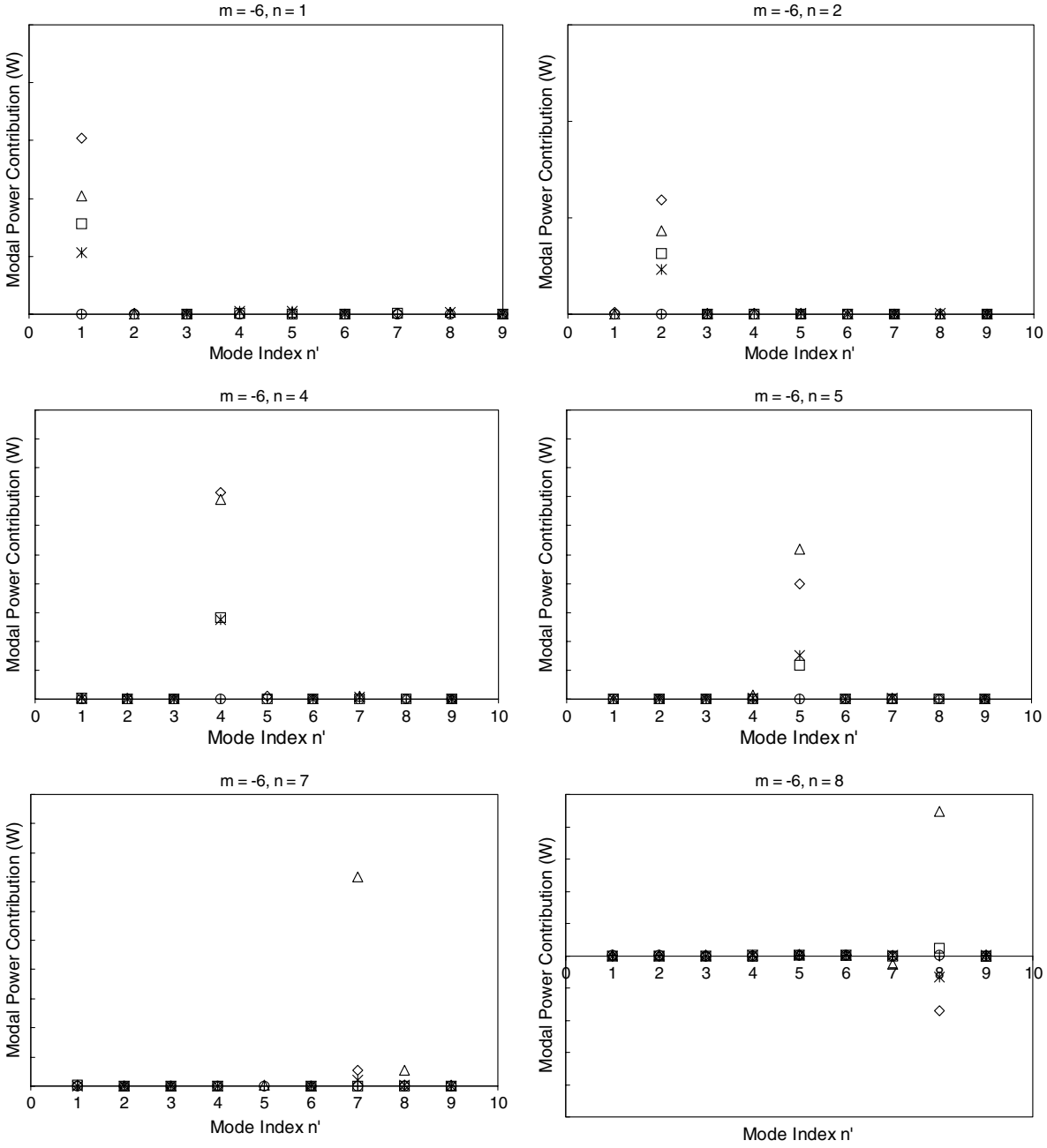

Fig. 16 Modal sound power contributions of downstream-propagating modes at 2BPF at cutback for the circumferential mode $m = -6$. The results of only six of the nine cuton radial modes are shown here.

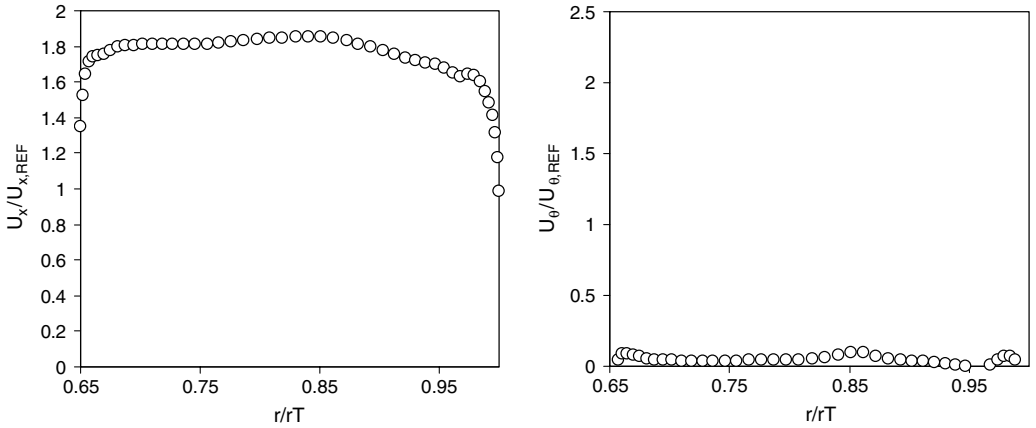

a) b)

Fig. 17 Circumferentially averaged mean flow radial profiles of a) axial and b) azimuthal nondimensional velocities downstream of the OGV trailing edge at cutback.

twice the blade passing frequency at cutback operation is plotted against axial distance downstream of the OGV trailing edge in Figs. 18 and 19 . These results corroborate the conclusion that at this frequency and for the nonuniform mean flow typical of this operating condition, the acoustic intensity can be regarded as locally conserved. A reasonable agreement between the sound power levels computed using Eq. (8) and using a uniform-flow model was achieved, although differences of up to 1 dB between the two models, and a higher rate of axial variation of the PWL for the uniform approximation could still be observed, particularly for $m = 52$.

2. Upstream Propagating Noise

In the case of upstream-propagating noise, similar results to those presented for the downstream-propagating noise regarding the comparison of the various postprocessing methods were found. The wave-splitting techniques proved more reliable than an acoustic analogy approach as they are less prone to errors due to the duct geometry variation and the construction of equivalent duct modes. Within the wave-splitting methods, a question still remains open on the effect of the mean flow nonuniformity and swirl. This was partly addressed in the previous section for downstream-propagating noise, but it is a more pressing issue upstream of the OGV, where flow swirl is far more significant. For this reason, the following paragraphs are devoted to the investigation of sound power for upstream-propagating noise.

In the two cases considered earlier for rear-arc interaction noise, the numerical calculation of the sound power showed that the acoustic energy flux is nearly conserved in nonuniform swirling flows that are typically found in the bypass duct (downstream of the OGV) of a modern turbofan engine. Also, the parts containing the mean flow azimuthal velocity component in the noninterference terms provided negligible contributions to the total sound power.

In the fan/OGV inter-rows region, the mean flow swirl upstream of the stator vanes is significantly larger than that in the bypass duct, therefore it is very interesting to study the effect of swirl on the sound power of upstream-propagating interaction noise. Figure 20 illustrates the significant swirl at the inlet of the bypass duct that the outlet guide vanes have to remove from the flow to turn it to an axial direction. The circumferentially averaged axial and azimuthal velocity components are nondimensionalized with two different reference values, $U_{x,\mathrm{ref}}$ and $U_{\theta,\mathrm{ref}}$ identical to those used in Fig. 17, so that a direct comparison can be made.

At the prescribed reduced frequency, based on half the stator chord, $\tilde{\omega} = c_x\omega/2U \sim 6.0$, only one counter-rotating spinning mode with a circumferential mode number $m = -6$ propagates upstream with the first six radial harmonics cuton. It is important to point out that the effect of mean flow swirl is crucial in determining the propagation of the acoustic waves. For example, at cutback operation, the fan tip speed is supersonic and in a uniform axial flow the upstream-propagating interaction mode $m = 52$ would be cuton. The effect of the mean flow swirl on this corotating spinning mode is to stop it from propagating away from the source.

As observed in the previous section, for the sound power to be conserved, the sum of the contributions due to the cross terms in Eq. (8) should equal zero. In practice, in any real turbomachinery application, due to the mean flow vorticity and nonuniformity, the sound power is not strictly conserved, but it can be retained locally conserved if the contributions due to the interference terms are insignificant. The contributions of each of the terms in Eq. (8) are summarized in Fig. 21.

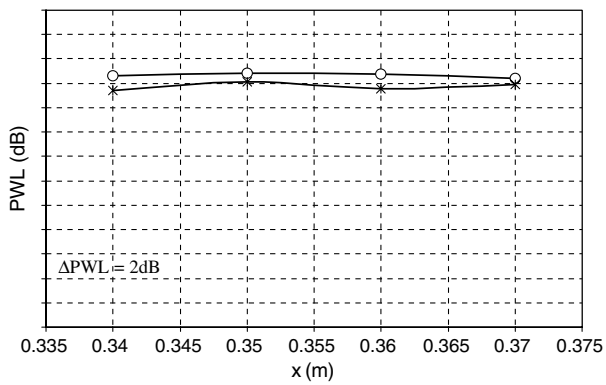

Fig. 18 Sound power variation with axial distance downstream of the OGV trailing edge at 2BPF at cutback for the circumferential mode $m = 52$. Modal sound power calculated using Eq. (8) (○) and computed for an equivalent uniform axial mean flow (*).

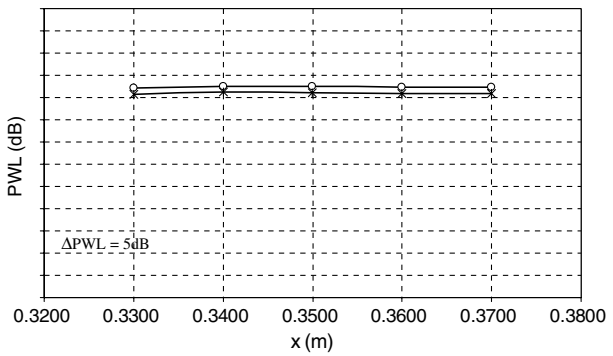

Fig. 19 Sound power variation with axial distance downstream of the OGV trailing edge at 2BPF at cutback for the circumferential mode $m = -6$. Modal sound power calculated using Eq. (8) (○) and computed for an equivalent uniform axial mean flow (*).

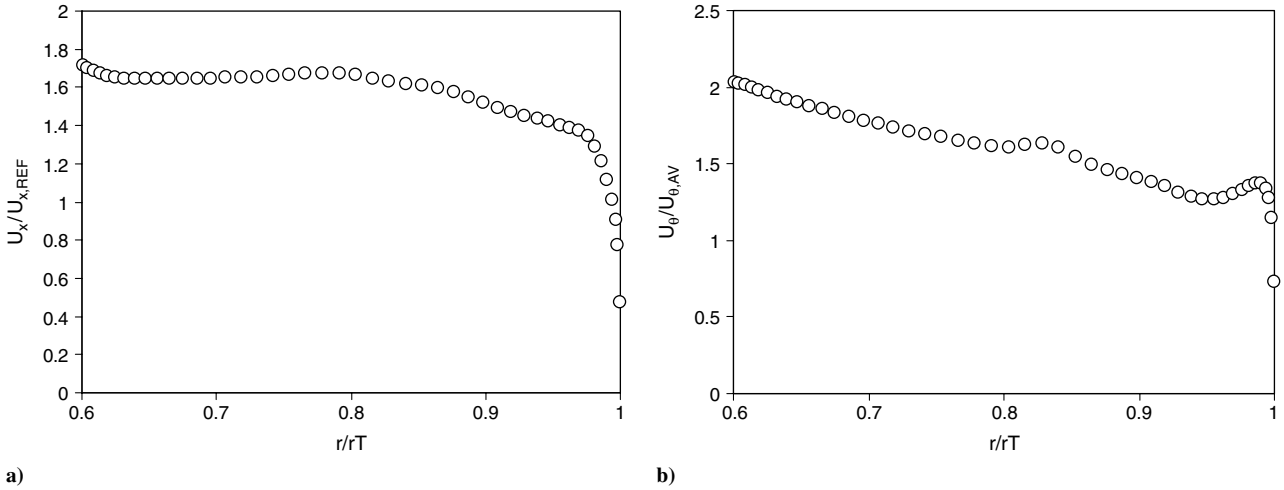

a) b)

Fig. 20 Circumferentially averaged mean flow radial profiles of a) axial and b) azimuthal nondimensional velocities upstream of the OGV leading edge at cutback.

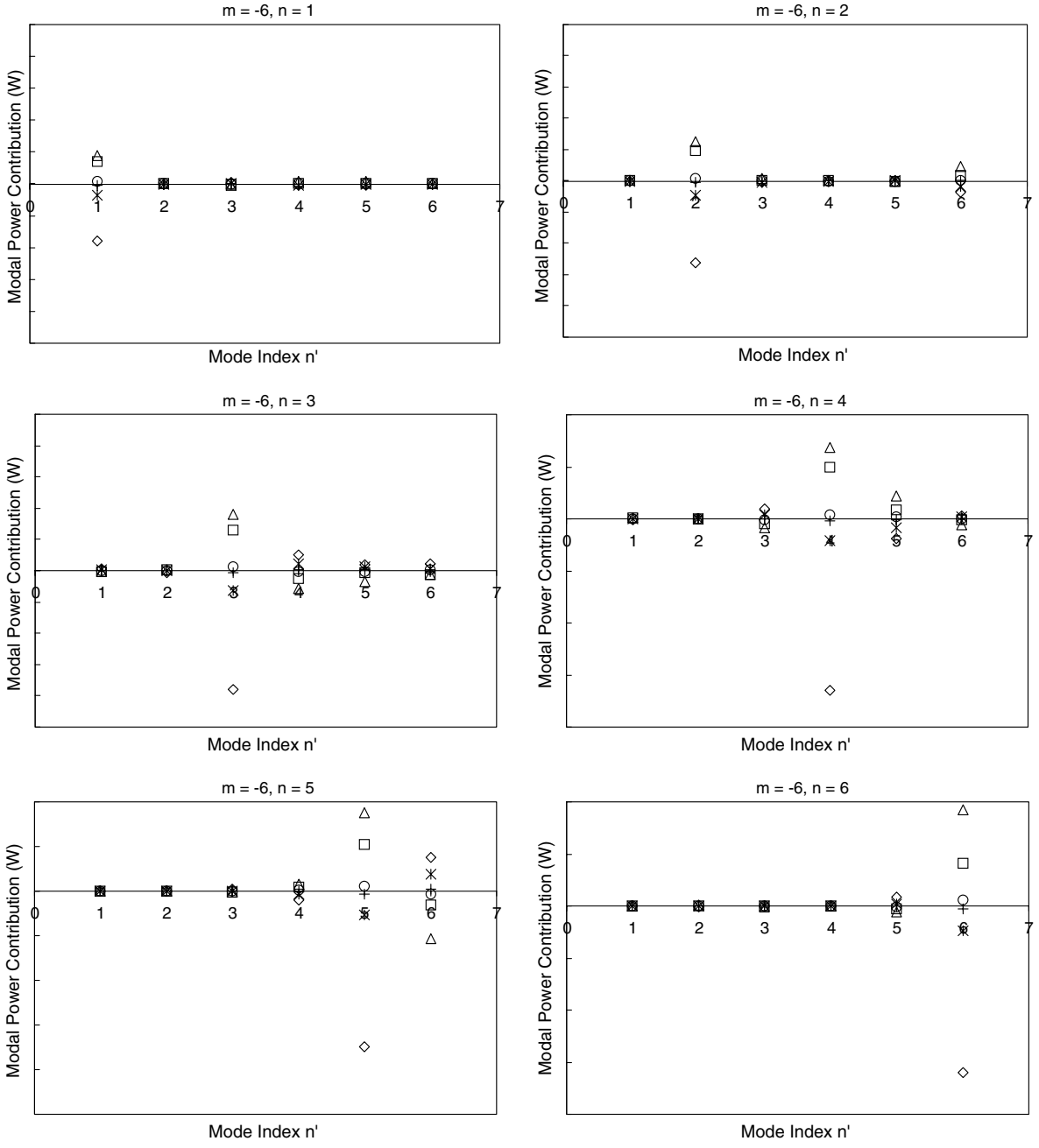

Fig. 21 Modal sound power contributions of upstream-propagating modes at 2BPF at cutback for $m = -6$.

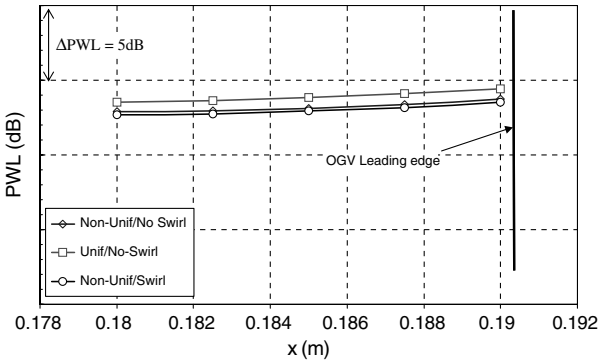

Fig. 22 Sound power variation with axial distance upstream of the OGV leading edge at 2BPF at cutback for the circumferential mode $m = -6$.

Upon a close examination of the results, it can be observed that for higher-order modes the contribution of the cross terms is larger for modes adjacent to the noninterference term ($n' = n \pm 1$), but they all nearly cancel out accounting for a negligible fraction of the total sound power.

In the noninterference terms, the dominant contribution is generally due to the first term of Eq. (8). The second and third terms also contribute significantly to the total sound power, but, by definition, they are always positive and for upstream-propagating waves they tend to reduce the emitted sound power.

It is also interesting to note that despite the significant mean flow swirl, the contribution due to the fifth and sixth terms appears very small. Although neglecting the mean flow swirl in the acoustic disturbance propagation and normal mode analysis of the flow would lead to large errors, the results presented thus far seem to indicate that dropping the terms related to the mean swirl in the modal sound power expression would produce small differences.

Figure 22 shows a comparison between the sound power calculated with the nonuniform modal expression and a simplified version computed for an equivalent uniform axial mean flow at this frequency. The effects of mean flow swirl and of the interference terms induced by the flow nonuniformity are therefore ignored not only in the modal sound power expression but, more important, also in the calculation of the eigenmodes.

In the majority of the current fan-noise prediction schemes, uniform axial mean flow duct modes are used, and, in light of the results presented thus far, it is interesting to address the following questions: How does the PWL change if uniform-axial-flow duct modes are considered? How does the PWL change if the mean flow effects and interference effects are neglected in the modal expression of the PWL for nonuniform swirling flows?

The results shown in Fig. 22 aim at answering these three questions. When the acoustic modes are computed for a nonuniform swirling flow, but the terms including the mean swirl and the interference effects are neglected in the modal expression of the sound power ($\diamond$ in Fig. 22), only a small difference is found, and it seems acceptable (although not advisable) to use such an approximation even for upstream-propagating noise in a fan-noise prediction scheme. When both the duct modes and the sound power modal expression are computed for a uniform axial flow ($\square$ in Fig. 22), the PWL seems still conserved, but its level is overpredicted by 1–2 dB, which is unacceptable in most cases. In conclusion, the results presented thus far indicate that it may be reasonable to neglect the effects of interference terms and mean flow swirl in the calculation of the sound power when a rigorous modal analysis of the mean flow is carried out. On the other hand, resorting to an equivalent uniform-axial-flow model is a poor approximation and can lead to large errors in the predictions.

V. Conclusions

This paper has presented a systematic study on the postprocessing methods available to date to extract tone-noise information from the source unsteady aerodynamic solutions. The assumptions at the base of an acoustic analogy based method, and different wave-splitting methods were assessed by use of numerical test cases of increasing flow and geometrical complexities.

The influence of the duct geometry and of nonuniform swirling flow on the accuracy and reliability of each method was investigated, and the results showed the shortcomings of an acoustic analogy approach, particularly in relation to the construction of equivalent duct modes in the presence of a duct geometry that varies along the engine axis. An acoustic integration strategy is especially prone to errors when the geometric changes occur in the source (OGV) region. On the other hand, the wave-splitting methods proved very accurate for all the cases considered, and no significant differences were observed between the L-R and 3P methods to calculate the modal amplitudes of the eigenfunctions.

The effect of a nonuniform swirling mean flow proved to be a source of error for all the methods under study. To detect this, the modal expression of the sound power for nonuniform swirling flows in the high-frequency limit was employed. This modal representation was used to assess the effects of mean flow swirl and interference terms arising from the nonorthogonality of the acoustic duct modes.

For the range of cases examined, it was found that the interaction between the mean flow and the acoustic waves for high reduced frequencies is weak, the interference effects are negligible, and, more important, the sound power is locally conserved.

From the results presented in this paper, it can be concluded that in the fan/OGV inter-row region it is important to account for the large mean swirl and nonuniformity of the flow in the computation of the acoustic modes, as these can vary substantially from those of a uniform flow, but also that a simplified expression for the sound power calculation can be adopted neglecting the interference terms contributions and the swirl components of the noninterference terms. In the prediction of rear-arc tone noise, a uniform-axial-flow approximation may be acceptable due to the low amount of residual swirl downstream of the bypass stator vanes for both the normal mode analysis and the sound power calculation. The importance of this conclusion also derives from the fact that numerous fan-noise prediction schemes compute the acoustic modes and sound power in a uniform axial mean flow without taking into consideration the contribution of the interference terms and/or of the mean flow swirl. It is nonetheless important to stress that there may be cases were interference terms are more significant, and it is recommended that the nonuniform modal expression should be used for both upstream- and downstream-propagating noise.

Acknowledgments

This work was supported by Rolls-Royce plc.. We gratefully acknowledge Rolls-Royce plc. for supplying the fan/bypass outlet guide vane test-case geometry and aerodynamics and the National Aerospace Laboratory (NLR, The Netherlands) for providing the Ffowcs Williams–Hawkings integral method.

References

[1] Atassi, O. V., "Computing the Sound Power in Non-Uniform Flow," *Journal of Sound and Vibration*, Vol. 266, No. 1, 2003, pp. 75–92. doi:10.1016/S0022-460X(02)01448-7

[2] Ffowcs Williams, J. E., and Hawkings, D. L., "Sound Generation by Turbulence and Surfaces in Arbitrary Motion," *Philosophical Transactions of the Royal Society of London, Series A: Mathematical and Physical Sciences*, Vol. 264, No. 1151, 1969, pp. 321–342. doi:10.1098/rsta.1969.0031

[3] Nijboer, R. J., "BLAIR–BLade Acoustic Integration Rountine: An Acoustic Radiation Code," National Aerospace Lab. Paper CR-2001-165, 2001.

[4] Wells, V. L., and Han, A. Y., "Acoustics of a Moving Source in a Moving Medium with Application to Propeller Noise," *Journal of Sound and Vibration*, Vol. 184, No. 4, 1995, pp. 651–663. doi:10.1006/jsvi.1995.0339

[5] Schulten, J. B. H. M., "Sound Generation by Ducted Fans and Propellers as a Lifting Surface Problem," Ph.D. Dissertation, University of Twente, Enschede, The Netherlands, 1993.

[6] Sutliff, D. L., "Coupling of Low Speed Fan Stator Vane Unsteady Pressures to Duct Modes: Measured vs. Predicted," NASA TM 1999-209050, May 1999.
[7] Sutliff, D. L., Bridges, J., and Envia, E., "Comparison of Predicted Low Speed Fan Rotor/Stator Interaction Modes to Measured," NASA TM-107462, 1997.
[8] Kerrebrock, J. L., "Small Disturbances in Turbomachine Annuli with Swirl," *AIAA Journal*, Vol. 15, 1977, pp. 794–803. doi:10.2514/3.7370
[9] Golubev, V. V., and Atassi, H. M., "Sound Propagation in an Annular Duct with Mean Potential Swirling Flow," *Journal of Sound and Vibration*, Vol. 198, 1996, pp. 601–616. doi:10.1006/jsvi.1996.0591
[10] Golubev, V. V., and Atassi, H. M., "Acoustic-Vorticity Waves in Swirling Flows," *Journal of Sound and Vibration*, Vol. 209, 1998, pp. 203–222. doi:10.1006/jsvi.1997.1049
[11] Tam, C. K. W., and Auriault, L., "The Wave Modes in Ducted Swirling Flows," *Journal of Fluid Mechanics*, Vol. 371, 1998, pp. 1–20. doi:10.1017/S0022112098002043
[12] Kousen, K. A., "Eigenmodes of Ducted Flows with Radially-Dependant Axial and Swirl Components," NASA CR-1999-208881, 1999.
[13] Cooper, A. J., and Peake, N., "Propagation of Unsteady Disturbances in a Slowly Varying Duct with Mean Swirling Flow," *Journal of Fluid Mechanics*, Vol. 445, 2001, pp. 207–234. doi:10.1017/S0022112001005559
[14] Nijboer, R., "Eigenvalues and Eigenfunctions of Ducted Swirling Flows," 7th AIAA/CEAS Aeroacoustics Conference, AIAA Paper 2001-2178, Maastricht, Netherlands, 28–30 May, 2001.
[15] Atassi, H. M., Ali, A. A., Atassi, O. V., and Vinogradov, I. V., "Scattering of Incident Disturbances by an Annular Cascade in a Swirling Flow," *Journal of Fluid Mechanics*, Vol. 499, 2004, pp. 111–138. doi:10.1017/S0022112003007031
[16] Heaton, C. J., and Peake, N., "Algebraic and Exponential Instability of Inviscid Swirling Flow," *Journal of Fluid Mechanics*, Vol. 565, 2006, pp. 279–318. doi:10.1017/S0022112006001698
[17] Heaton, C. J., and Peake, N., "Acoustic Scattering in a Duct with Mean Swirling Flow," *Journal of Fluid Mechanics*, Vol. 540, 2005, pp. 189–220. doi:10.1017/S0022112005005719
[18] Wilson, A. G., "A Method for Deriving Tone Noise Information from CFD Calculations on the Aeroengine Fan Stage," *NATO RTO-AVT Symposium on Developments in Computational Aero- and Hydro-Acoustics*, Oct. 2001.
[19] Ovenden, N. C., and Rienstra, S. W., "Mode-matching Strategies in Slowly Varying Engine Ducts," *AIAA Journal*, Vol. 42, No. 9, 2004, pp. 1832–1840. doi:10.2514/1.3253
[20] Vilenski, G., "Mode Matching in Engine Ducts with Vortical Flows," 12th AIAA/CEAS Aeroacoustics Conference, AIAA Paper 2006-2584, 2006.
[21] Moinier, P., and Giles, M. B., "Eigenmode Analysis for Turbomachinery Applications," *Journal of Propulsion and Power*, Vol. 21, No. 6, 2005, pp. 973–978. doi:10.2514/1.11000
[22] Giacché, D., "Design and Optimisation of Low Noise OGV," Ph.D. Dissertation, University of Cambridge, Cambridge, England, U.K., 2009.
[23] Myers, M. K., "Transport of Energy by Disturbances in Arbitrary Steady Flows," *Journal of Fluid Mechanics*, Vol. 226, 1991, pp. 383–400. doi:10.1017/S0022112091002434
[24] Dahl, M. D., "Third Computational Aeroacoustics (CAA) Workshop on Benchmark Problems," NASA CP-2000-209790, Aug. 2000.
[25] Schulten, J. B. H. M., and Namba, M., "Numerical Results of Lifting Surface Theory—Cat. 4 Benchmark Problem 3rd CAA Workshop," National Aerospace Lab. TP-2000-013, Amsterdam, 2000.
[26] Moinier, P., Giles, M. B., and Coupland, J., "Three-Dimensional Non-Reflecting Boundary Conditions for Swirling Flows in Turbomachinery," *Journal of Propulsion and Power*, Vol. 23, No. 5, 2007, pp. 981–986. doi:10.2514/1.22117
[27] Wilson, A. G., "Application of CFD to Wake/Aerofoil Interaction Noise —A Flat Plate Validation Case," 7th AIAA/CEAS Aeroacoustics Conference, AIAA Paper 2001-2135, May 2001.
[28] Elhadidi, B., "Sound Generation and Propagation in Annular Cascades with Swirling Flows," Ph.D. Dissertation, University of Notre Dame, Notre Dame, IN, 2002.

J. Astley
Associate Editor